Climate and Prehistoric Migration*

Peter Huybers Marco Tabellini Charles A. Taylor Francesco Toti

January 2026

Abstract

How did climate shape human migration before modern states, markets, and borders? We study prehistoric migration over the past 10,000 years using ancient DNA to measure population movements directly. Building on recent advances in genetics, we use identity-by-descent links between ancient individuals to construct a panel of bilateral migration flows across Eurasia, analogous to migration datasets commonly used in economics but measured from genetic relatedness. We combine these flows with high-resolution climate data to study how environmental similarity shaped migration decisions over the very long run. We document three main findings. First, migration flows decline with climate distance, as measured by the difference in growing degree days between origins and destinations. Second, these patterns are stronger in farming and pastoral societies than among foragers, pointing to subsistence-based mechanisms. Third, migration responds to climate change: populations exposed to warming migrate toward cooler destinations, suggesting that local adaptation was costly and that migration served as an important margin of adjustment. Together, the results provide new evidence on the ecological foundations of human mobility in deep history.

Keywords: Migration, prehistory, climate, ecology.

JEL codes: N50, O13, Q54, Z13

*Huybers: Department of Earth and Planetary Science, Harvard University. Tabellini: Harvard Business School and NBER. Taylor: Harvard Kennedy School and NBER. Toti: University of Michigan, Ann Arbor. We thank Gabrielle Lévy for excellent research assistance. All remaining errors are ours.

1 Introduction

For most of human history, migration was not a response to wage differentials, institutions, or political borders, but to the spatial distribution of ecological opportunities and risks. Hunter-gatherers, early farmers, and pastoralists all depended on local ecological conditions, though the specific constraints differed: farmers were bound to thermal regimes governing crop growth, while foragers and pastoralists were more sensitive to water availability and pasture conditions. A central insight of anthropology and archaeology is that mobility strategies were organized around seasonal patterns: where food could be produced, stored, or accessed during the growing season, and how predictable those conditions were from one place to the next (Lee and DeVore, 1968). In mid- and high-latitude environments, where the length and intensity of the warm season constrains biological productivity, moving into a region with an unfamiliar thermal regime could threaten subsistence itself. Prehistoric migration was not merely about distance or terrain, but about whether new environments were ecologically legible—that is, whether their thermal structure supported the specific biotic systems people already knew how to exploit.

Findings in archaeology, paleoecology, and paleoclimatology provide support for this seasonal perspective. Quantitative studies of crop dispersal show that thermal thresholds and growing-season length constrained where early farmers could move, shaping migration routes, settlement patterns, and even the adoption of mixed subsistence strategies (Guedes and Butler, 2014; Castiello et al., 2025). Other work emphasizes that climate influences migration indirectly, through its effects on vegetation and land cover rather than through simple "warm versus cold" regimes (Racimo et al., 2020). At the same time, paleoclimate evidence shows that major migration episodes often occurred under very different mean climate states, complicating deterministic narratives and pointing instead to the importance of seasonal structure, variability, and risk (Tierney et al., 2017). Despite these insights, much of this literature remains necessarily indirect: it infers mobility from settlement locations, crop assemblages, or environmental reconstructions, rather than from observed movements of people themselves. As a result, we still lack a population-level test of whether humans systematically moved along corridors of seasonal climate familiarity over the long run.

This paper brings new evidence to bear on this question using ancient human DNA that tracks population ancestry across space and time. By observing where the ancestors of individuals appear and reappear across Western Eurasia over the past 10,000 years, we can measure migration flows rather than infer them. This is made possible by recent advances in population genetics (Reich, 2018). In particular, long identity-by-descent (IBD) segments in ancient DNA reveal recent genealogical links between individuals who lived hundreds or even

thousands of kilometers apart. Because recombination rapidly breaks down these segments over generations, their length provides a tight bound on the recency of shared ancestry. Ringbauer et al. (2024) introduce an algorithm (ancIBD) that reliably detects IBD segments even in low-coverage ancient genomes, allowing biological relatedness to be traced at time horizons of centuries across thousands of individuals.

We use these pairwise genealogical links to construct a panel of migration flows across Western Eurasia, broadly defined to match the spatial coverage of existing ancient DNA datasets. We discretize space into geographic cells of $1^\circ \times 1^\circ$ latitude–longitude and time into 500-year windows, and define migration between two locations as the count of individual pairs sharing IBD segments linking individuals buried in different places but close in time. Aggregating these links yields a migration matrix that captures the intensity of population movement across space and time, analogous to modern migration datasets commonly used in economics but measured directly from genetic relatedness. We then combine this genetically derived migration matrix with high-resolution modern climate data and paleoclimate reconstructions to test whether prehistoric migration was systematically shaped by similarity in local climate and ecological factors.

We adopt a gravity framework commonly used in the international trade literature (Anderson and Van Wincoop, 2003), and express bilateral migration as a function of physical distance. Building on recent work that documents the importance of climate matching for migration in the modern era (Obolensky et al., 2024), we augment the baseline gravity specification by introducing climate distance between origin and destination.

Our preferred measure of climate distance is the absolute difference in cumulative growing-degree days above 10°C, which captures biologically relevant heat accumulation for plant growth and animal productivity (Schlenker and Roberts, 2009; Butler and Huybers, 2013). Unlike seasonal or annual temperature averages, degree days summarize both the intensity and duration of warmth during the growing season, and are therefore closely aligned with subsistence constraints emphasized in anthropology and archaeology. Paleoclimate evidence further shows that growing-season heat accumulation can evolve independently of mean summer temperatures over the Holocene, making degree days a more appropriate measure of climatic similarity in deep history (Mourshed, 2012; Marsicek et al., 2018).

We find that climate distance reduces migration. Migration flows decline sharply with differences in cumulative growing-degree days above 10°C between origin and destination, while temperature distance outside the growing season (i.e., winter temperature) plays a smaller role. Precipitation distance also consistently reduces migration, with effects that are stable across specifications and—unlike growing-degree days—do not attenuate substantially when controlling for geographic distance, suggesting that water availability represented an

independent ecological constraint on prehistoric mobility. Soil characteristics emerge as another important dimension of ecological matching: differences in soil quality between origin and destination significantly reduce migration flows, consistent with the idea that agricultural knowledge was tied to specific edaphic conditions. Our preferred specification includes origin fixed effects, destination fixed effects, and era fixed effects at 500-year intervals, along with a set of bilateral controls. Era fixed effects absorb aggregate shifts in migration intensity, while origin and destination fixed effects account for persistent differences in population size, mobility propensity, and data density across locations. The results are also robust to interacting origin and destination fixed effects with era fixed effects, which absorb time-varying push and pull factors such as changes in local population size, subsistence systems, environmental conditions, or data coverage.

A natural concern is the spatial correlation of climate: nearby locations tend to have similar temperatures, and migrants tend to move short distances. To address this, we flexibly control for geographic distance by including both distance and distance squared. This reduces the magnitude of the estimated effect of climate distance but leaves its precision unchanged. Our results also hold if we instead use a travel cost measure that accounts for terrain difficulty and water barriers. We compute least-cost paths using a transition matrix derived from slope (from elevation data) and water body coverage, where steep terrain and water crossings increase effective travel distance (Figure A4). This matters because straight-line distance may substantially understate the difficulty of crossing mountain ranges or bodies of water that shaped prehistoric mobility corridors. Our preferred specification also includes bilateral controls capturing precipitation, soil, and elevation distance. We discuss additional robustness checks below, after presenting the results.

We subject these findings to an extensive battery of robustness checks, summarized in Table 4. The baseline GDD effect is robust to: (i) restricting the sample to moves of at least 100 km; (ii) analyzing horizontal (east-west) and vertical (north-south) movements separately; and (iii) using alternative dependent variables including counts of IBD segments above 12 cM and 16 cM thresholds, as well as sum of segment lengths. Across all specifications, the GDD coefficient remains negative and statistically significant, with magnitudes ranging from -0.12 to -0.30. Notably, horizontal moves show patterns similar to the full sample, while vertical moves—which are far fewer in number—show weaker but directionally consistent effects. The robustness across IBD thresholds suggests that climate matching operates similarly for both recent genealogical connections (longer segments) and somewhat more distant relationships (shorter segments). The precipitation coefficient is similarly robust, remaining negative and significant (-0.008 to -0.018) across all specifications except vertical moves—consistent with the predominantly east-west orientation of precipitation gradients

in Western Eurasia.

According to our estimates, increasing the distance in growing-degree days by 1,000 reduces migration flows by about 20%. For reference, a difference of 1,000 growing-degree days is equivalent to a 5°C higher mean daily temperature sustained over a standard 200-day growing season—that is, roughly 5°C more warmth on each day above the 10°C threshold. From an agronomic perspective, this represents a substantial climatic shift, comparable to the difference between a cool-temperate cropping system such as wheat (which requires on the order of 1,500 growing-degree days) and a warm-temperate system such as maize (which requires closer to 2,500 growing-degree days).

These patterns are consistent with the idea that migration costs in prehistory were driven primarily by the specificity of subsistence technologies. Success in pre-industrial societies relied on deep knowledge of local biotic cycles—when to plant, when to herd, and what to forage. These cycles are regulated by accumulated thermal time. The results align with anthropological accounts emphasizing seasonal resource scheduling (Lee and DeVore, 1968), as well as with archaeological evidence that the spread of farming and herding was constrained by growing-season length and thermal thresholds (Guedes and Butler, 2014; Castiello et al., 2025). These findings highlight the importance of climate-specific human capital as a mechanism driving migration decisions (Obolensky et al., 2024): individuals possess a set of climate-specific skills and knowledge whose transferability declines with climate distance (e.g., pastoralists from a warm climate lack skills to keep their livestock alive in a blizzard, whereas cold weather pastoralists cannot manage the intense thermal stress and parasite load of a hot summer).

Consistent with this interpretation, we find that the response to growing-degree days distance is stronger among populations with greater reliance on farming and pastoralism, as compared to predominantly foraging societies. In contrast, we find no corresponding heterogeneity along the winter temperature dimension. This pattern reinforces the view that growing-season conditions were the primary constraint shaping migration decisions, particularly in societies whose subsistence depended directly on crops or managed livestock. For foragers, whose livelihoods were less tightly linked to fixed growing seasons, climate matching along the summer dimension appears to have been less salient.

A key advantage of our setting is that it spans nearly 10,000 years, allowing us to examine how the relationship between climate similarity and migration evolves over time. We find that climate matching is weaker during periods of warming. One interpretation is that warming relaxes ecological constraints on subsistence, expanding the range of environments in which crops, livestock, and vegetation regimes can be sustained. As growing seasons lengthen and thermal constraints ease, the costs of moving into climatically unfamiliar areas

fall, reducing the penalty associated with climate mismatch. In this sense, climate matching matters most when environments are near subsistence thresholds, whereas periods of warming attenuate these constraints by making a broader set of destinations viable. This pattern is consistent with archaeological evidence that phases of climatic amelioration are associated with range expansions, ecological experimentation, and reduced sensitivity to local growing-season conditions (Richerson et al., 2001; Dow et al., 2009; Olsson, 2024).

The long time span of our setting, together with substantial climate change over the Holocene (Marcott et al., 2013), allows us to ask whether and how individuals adapted to changing climatic conditions. In particular, we examine whether migration served as a mechanism to offset local climate change. We compare the climate experienced by individuals' ancestors at their origin with the climate at their eventual destination, focusing on pairs of related individuals observed within 500 years. We then relate changes in temperature over time at the origin to changes in temperature over space induced by migration.[1] Intuitively, if individuals respond to local warming by relocating toward places that match their ancestral ecological niche, then increases in average temperature at the origin should be associated with migration toward cooler destinations.

We find evidence that migration acted as an adaptive response to climate change. When origins experience warmer summers, individuals systematically migrate toward destinations with cooler summer temperatures, partially offsetting local warming. These patterns mirror our earlier findings on bilateral migration flows and highlight the central role of growing-season conditions in shaping mobility decisions. These results imply that local adaptation to climate change was costly or constrained. If adaptation through changes in crops, technologies, or practices were easy or immediate, individuals would have had little incentive to relocate in response to gradual warming. Instead, the systematic migration responses we document indicate that migration served as a key margin of adjustment when local subsistence systems were slow to adapt. This interpretation is consistent with evidence that preindustrial subsistence depended tightly on growing-season conditions and that adapting to new thermal regimes required substantial changes in crops, knowledge, or social organization (Richerson et al., 2001; Ashraf and Michalopoulos, 2015).

Taken together, our findings provide systematic, population-level evidence for long-standing insights in anthropology, archaeology, and paleoecology that emphasize the role of ecological constraints and climate conditions in shaping human mobility and settlement patterns (Lee and DeVore, 1968; Guedes and Butler, 2014; Racimo et al., 2020; Castiello

[1]Because paleoclimate reconstructions do not permit reliable measurement of within-year temperature variation or growing-degree days at fine temporal resolution, this analysis uses average annual temperature as a coarser proxy for climatic conditions.

et al., 2025). Related is Diamond (1997)'s argument that the relatively uniform east–west transects of Eurasia enabled the diffusion of people, crops, and inventions—an idea supported by work using DNA data from modern populations to show that distance in latitude explains more genetic variation than longitude (Ramachandran and Rosenberg, 2011).

Our evidence on migration responses to climate change also complements work in cultural evolution that highlights the slow, cumulative nature of local adaptation and the costs of acquiring ecologically specific subsistence knowledge, particularly in seasonal environments (Henrich, 2004; Boyd et al., 2011; Nunn, 2021).

Within economics, our paper contributes to the literature that studies how environmental conditions and subsistence systems shape long-run economic and social outcomes. Michalopoulos (2012) shows that variation in land quality and terrain fosters ethnolinguistic differentiation by limiting population movement. Fenske (2014) documents that ecological diversity promotes trade across zones and supports the emergence of centralized states in pre-colonial Africa. Ashraf and Michalopoulos (2015) link climatic variability to the diffusion of agriculture, while Giuliano and Nunn (2021) show that environmental stability across generations fosters cultural persistence. Matranga (2024) highlights the role of climatic seasonality in the transition from mobility to sedentarism and the invention of agriculture.

A primary contribution of this paper is to introduce to this literature an approach and dataset that captures prehistorical migration flows. Building on seminal work in genetics (Reich, 2018; Ringbauer et al., 2024), we derive population-level bilateral migration flows from ancient DNA and analyze prehistoric mobility using the same empirical framework—gravity-style flows, distance frictions, and origin–destination structure—that economists routinely apply to modern migration. In doing so, we provide evidence on how populations adjusted to environmental constraints and climate change in deep history, and document systematic patterns linking migration to seasonality, subsistence systems, and long-run climatic change. These findings complement theories that emphasize environmental forces, population dynamics, and adaptation in shaping long-run development (Galor and Moav, 2002; Ashraf and Galor, 2013; Galor and Özak, 2016).

Finally, our paper complements a recent literature that documents the role of climate similarity in shaping migration and development in historical and modern settings. Obolensky et al. (2024) document climate matching in U.S. migration between 1850 and 2020, and show that climate mismatch slowed economic growth over the 1880–1920 period. Nicolò et al. (2026) provide evidence in support of Alfred Crosby's hypothesis that Europeans thrived in the Neo-Europes because of environmental similarity between origin and destination (Crosby, 1986). We contribute to this literature by pushing the analysis back into prehistory and by showing that climate similarity matters primarily along seasonal dimensions. In contrast

to existing work, which focuses on mean annual temperature, our results highlight the central role of growing-season conditions in shaping migration decisions long before modern institutions or labor markets.

2 Data

This section describes the main datasets used in the analysis. Table 1 presents summary statistics for the main variables.

2.1 Migration flows from Ancient DNA

Prehistoric migration patterns are difficult to study because direct records of individual movements do not exist. To overcome this limitation, we rely on ancient DNA (aDNA) data, which make it possible to infer population movements indirectly from genealogical relationships observed across space and time. Our approach builds on recent advances in population genetics that allow researchers to identify pairs of individuals who share a recent common ancestor and to use the spatial separation of such pairs as evidence of past mobility (Reich, 2018).

The key object in our analysis is identity-by-descent (IBD). Two individuals share an IBD segment when they inherit the same stretch of DNA from a common ancestor without recombination. Because recombination breaks chromosomes into shorter segments in each generation, the length of an IBD segment, as measured in centimorgan (cM), provides information about the recency of the shared ancestor: segments 8cM or longer segments imply more recent genealogical links. In modern genetic data, IBD has been widely used to study recent population structure and migration (Palamara et al., 2012; Ralph and Coop, 2013). Until recently, however, its use in ancient DNA was limited by the low genomic coverage of ancient samples.

Ringbauer et al. (2024) develop a method, ancIBD, that overcomes this limitation by reliably detecting IBD segments even in low-coverage aDNA. Applying this method to a large collection of ancient genomes from Western Eurasia, they identify thousands of pairwise genealogical links spanning distances of up to several hundred kilometers and time horizons of a few hundred years. We rely on their publicly available IBD calls and associated metadata as the foundation of our migration measure. We interpret a pair of related individuals buried in different locations as evidence that at least one movement occurred between those locations within the genealogical window implied by the IBD segment greater than 8cM. This interpretation does not require observing the migrant directly: even if both individuals are

buried at their places of birth, the existence of a recent genealogical link across space implies migration by an intermediate ancestor. In this sense, IBD captures population movement rather than individual travel and is well suited to studying migration in deep history.

To focus on movements that are plausibly interpretable as migration rather than long-run population replacement, we restrict attention to pairs of individuals who lived within 1,000 years of one another. We further restrict the sample to individuals dated to after 10,000 BCE, a period for which both the density of aDNA samples and the quality of paleoclimate reconstructions (discussed below) improve substantially (Marcott et al., 2013; Reich, 2018). For each qualifying pair, we observe the burial locations of the two individuals, the time difference between them, and the total length of IBD segments they share. We aggregate these pairwise genealogical links to construct population-level migration flows at the gridcell level. Specifically, we discretize space into $1^o \times 1^o$ latitude–longitude cells and time into 500-year windows. For each origin–destination–period triple, we define migration intensity as the count of individual pairs sharing at least one IBD segment of 8 cM or longer, linking individuals buried in different cells but within the same time window.

For robustness, we also run our analysis using non-aggregated pair-wise genetic flows between individuals.

2.2 Climate

Modern. Our baseline analysis uses modern climate data, which offer substantially higher spatial resolution and richer within-year variation than currently available paleoclimate reconstructions. We measure local climate conditions using data from two sources. First, we use the ERA5, a global atmospheric reanalysis produced by the European Centre for Medium-Range Weather Forecasts (ECMWF), providing consistent, gridded fields of key variables like temperature and precipitation at hourly resolution from 1940 to present (Hersbach et al., 2020). We also use monthly climate data from TerraClimate (Abatzoglou et al., 2018), a widely used, high-resolution (≈4 km) global climate dataset constrained by a hydro-climate model that provides surface water and energy balance variables from 1958 onward.

Specifically, we compute average annual temperature and precipitation for each $1^o \times 1^o$ grid cell over the period 1960–2000, as well as summer (April–September) and winter (October–March) averages. In addition, we use the daily ERA5 data to construct measures that capture growing-season conditions and seasonal exposure, including cumulative growing-degree days above 10°C—which summarize biologically relevant heat accumulation for plant growth and animal productivity.

Paleoclimate. We complement modern climate data with paleoclimate reconstructions both as a robustness check and to exploit temporal variation in climate over the Holocene. We use gridded reconstructions of annual mean surface air temperature from the NOAA World Data Service for Paleoclimatology, based on the Last Glacial Maximum Reanalysis (LGMR) product (Osman et al., 2021). This dataset provides temperature estimates at 200-year intervals and combines information from marine geochemical proxies—such as oxygen isotope ratios in carbonate ($\delta^{18}O_c$), Mg/Ca ratios, TEX_{86} (Tetraether Index), and UK'_{37} (Alkenone Unsaturation Index) with simulations from the Community Earth System Model (iCESM1.2 and iCESM1.3).[2] The resulting gridded temperature data have a spatial resolution of $1.9^o \times 2.5^o$, which we aggregate to the $1^o \times 1^o$ grid used to measure migration flows.

Paleoclimate reconstructions of temperature are highly correlated with modern temperature patterns and are generally regarded as reliable representations of long-run spatial and temporal variation in temperature. By contrast, precipitation reconstructions remain more uncertain and contested in the paleoclimate literature (Smerdon et al., 2017). For this reason, we rely on modern precipitation data as our primary source for precipitation throughout the analysis.

2.3 Soil, topography and other environmental data

We obtain information on elevation and soil characteristics such as soil pH, soil water holding capacity, organic carbon, bulk density, and clay content from Hengl (2018b); Hengl and Wheeler (2018); Hengl and Gupta (2019); Hengl (2018a). We combine these soil variables into a composite soil quality index using principal component analysis, which captures the primary dimension of variation in edaphic conditions across Western Eurasia. In Figure A1, we plot the grid cell-level correlation between temperature and precipitation and each of these soil and topographic variables.

We also construct measures of diurnal temperature range—the difference between daily maximum and minimum temperatures—from TerraClimate (Abatzoglou et al., 2018). This variable captures temperature volatility, which is relevant for crop stress, frost risk, and livestock management, and may represent a distinct dimension of climate matching beyond mean temperatures.

For the heterogeneity analysis, we obtain historical land use data from the HYDE 3.2

[2]Oxygen isotope ratios in foraminifera shells ($\delta^{18}O_c$) reflect past sea surface temperatures and global ice volume, with lower values indicating warmer conditions. Mg/Ca ratios in these shells increase with temperature. TEX_{86}, based on lipids produced by marine archaea, provides an additional temperature proxy, particularly useful when carbonate records are sparse. UK'_{37}, derived from alkenones produced by coccolithophores, captures sea surface temperatures through temperature-sensitive variation in molecular unsaturation.

database (Klein Goldewijk et al., 2017), which provides gridded estimates of cropland and pasture area over the Holocene at 500-year intervals. We classify origin locations as predominantly forager, pastoral, or farming based on the relative intensity of cropland versus grazing land in each grid cell and time period.

Geographic distance between grid cell centroids is computed using the Haversine formula, which accounts for the curvature of the Earth. We include both distance and distance squared in our specifications to allow for a flexible, non-linear relationship between migration flows and spatial separation.

3 Descriptive Evidence

In this section, we present descriptive evidence that brings together the migration and climate data described above.

Migration. Figure 2 visualizes the ancient DNA derived migration flows across Western Eurasia in four panels—one for each time period, from 5000BCE to 2000BCE. Each panel displays links between locations where genetically related individuals are observed.[3] The figure reveals substantial variation in migration intensity across periods, as well as pronounced shifts in migration routes over millennia.

One pattern that stands out is the prevalence of "horizontal" movements, with migration occurring more frequently along east–west axes than along north–south ones. Such east–west mobility gradient has been documented in recent work using genealogical links in ancient DNA (Ringbauer et al., 2024). While this partly reflects the geography of the region under study, it is also consistent with the idea that migrants tended to move toward climatically similar environments. Such horizontal sorting has been documented in other historical and modern contexts (Steckel, 1983; Obolensky et al., 2024; Diamond, 1997), and our analysis below confirms that prehistoric migration was likewise shaped by climate similarity.

In addition to reconstructed migration flows, ancient DNA data allow us to observe rich variation in the spatial distribution of cultural groups over time. Groups are classified based on Ringbauer et al. (2024)'s classification by population, by homogenizing and rationalizing some groups into tighter categories. Figure A2 plots the locations of major cultural groups represented in the sample. Each panel corresponds to a distinct group, together with ap-

[3]For visualization purposes, we define two individuals as genetically related only if they share at least 16 centimorgans (cM) of identity-by-descent segments. In the main analysis, we use a lower threshold of 8 cM—the minimum length at which the method in Ringbauer et al. (2024) reliably identifies IBD; as discussed below, our results are robust to alternative IBD length cutoffs. The higher threshold used in this figure serves solely to reduce visual clutter.

proximate date, including early farming societies, steppe-associated populations, and later Bronze and Iron Age groups. The figure highlights both continuity and change in the geographic footprint of cultural groups, with some remaining spatially concentrated over long periods and others spreading rapidly across large parts of Western Eurasia.

Several broad patterns are apparent. Early farming groups are initially clustered in relatively narrow regions, while later steppe-associated groups exhibit much wider geographic dispersion. Over time, cultural groups increasingly overlap in space, reflecting repeated episodes of migration, interaction, and admixture. These patterns are in line with existing archaeological and genetic accounts emphasizing large-scale population movements and cultural diffusion in prehistoric Eurasia (Lazaridis et al., 2014; Allentoft et al., 2015), and underscore that prehistoric mobility was closely intertwined with the expansion and interaction of distinct cultural groups. Figure 5 builds on this information by plotting migration flows separately for each major cultural group. The figure reveals substantial heterogeneity in mobility across cultural contexts, both in the scale of movement and in its spatial orientation.

A particularly striking example is provided by the Yamnaya and related early steppe groups, originating in the Pontic–Caspian steppe during the late Neolithic and early Bronze Age, and widely regarded as central to the spread of Indo-European languages (Reich, 2018). Migration flows associated with the Yamnaya exhibit a pronounced east–west orientation, spanning large distances across the Eurasian steppe belt. This horizontal pattern is consistent with archaeological and genetic evidence documenting long-distance movements along ecologically similar steppe environments (Anthony, 2007; Haak et al., 2015) and with recent ancient DNA evidence showing extensive east–west genealogical connectivity across the Eurasian steppe (Ringbauer et al., 2024). More broadly, the figure highlights that the spatial structure of migration differs across cultural groups. Farming societies tend to display more localized movements, while steppe-associated groups exhibit wider-ranging and more directional mobility. These descriptive patterns motivate the heterogeneity analysis below, where we examine how migration responses to climate similarity vary across subsistence systems and cultural contexts.

Migration distance over time. Figure 6 documents a striking temporal pattern in the geographic scale of migration. The figure plots the average distance between genetically related individuals over time, computed at 250-year intervals from 6000 BCE to the present. Prior to approximately 3250 BCE, the average distance between related individuals remained relatively stable, fluctuating between 500 and 900 kilometers. After this date, migration distances increased dramatically, peaking at over 2,000 kilometers around 2500 BCE be-

fore gradually declining toward approximately 1,300 kilometers by the Roman period. The vertical dashed line marks the approximate date of wheel and wagon adoption in the Pontic-Caspian steppe region (Anthony, 2007). The timing of the increase in migration distance closely coincides with this technological innovation, suggesting that wheeled transport substantially expanded the geographic reach of population movements. This pattern complements the cultural evidence on Yamnaya expansion discussed above and underscores the role of transportation technology in enabling long-distance migration during the Bronze Age.

Climate. We next document the spatial distribution of key climate variables across the study region. Figure 1 displays two measures of modern climate at 1° resolution. Panel A shows cumulative growing degree days above 10°C, derived from ERA5 reanalysis data, which captures biologically relevant heat accumulation during the growing season—a key determinant of agricultural productivity and vegetation patterns. Panel B shows mean monthly precipitation from TerraClimate. Both variables exhibit pronounced spatial gradients, with growing degree days declining sharply with latitude and precipitation varying substantially across longitudinal bands.

A defining feature of the Holocene is that it was marked by substantial fluctuations in average temperature over time (Marcott et al., 2013). Figure 4 illustrates these long-run dynamics by plotting reconstructed average temperature in the study region from 8,000 BCE to 0, highlighting alternating phases of warming and cooling. Figure 3 shows the spatial distribution of paleoclimate temperature reconstructions from marine proxy data (Osman et al., 2021). Panel A displays reconstructed temperature for an illustrative period (2950 BCE), while Panels B and C show how temperature changed over time: Panel B plots the change between 5000 and 4000 BCE, a period characterized by broad warming, while Panel C presents the corresponding change between 3500 and 2000 BCE, a period of net cooling.

The maps reveal pronounced spatial heterogeneity in temperature change: some regions experienced substantial warming, others cooled, and many saw relatively muted change over the same period. Even within the same broad latitude bands, temperature shifts varied markedly across locations. This combination of long-run temporal change and fine-grained spatial heterogeneity generates meaningful variation in the climatic conditions faced by populations over time, which we exploit in the analysis below.

4 Climate Matching and Migration

4.1 Empirical Strategy

Our empirical analysis builds on the origin–destination migration panel constructed from ancient DNA data, as described in Section 2.1. The unit of observation is a pair of locations in a given (500-year) period. For each period, we consider the set of grid cells that contain at least one observed individual in that period or in the immediately subsequent period. Restricting attention to this set ensures that origins and destinations correspond to locations that were plausibly occupied and connected at that point in time, while excluding regions for which migration flows are not meaningfully defined. We then construct all origin–destination pairs among these cells, yielding a panel of bilateral migration flows that includes both positive flows and imputed zeros for pairs of locations between which no genealogical links are observed.

To study how environmental similarity shapes migration, we estimate gravity-style models of migration, building on the trade literature (Anderson and Van Wincoop, 2003). In this framework, bilateral migration flows depend on origin-specific and destination-specific factors that vary over time, as well as on bilateral frictions that are constant within a period. Following Obolensky et al. (2024), we augment the standard gravity specification with measures of climate distance between origin and destination, alongside physical distance.

Formally, for origin o, destination d, and period t, we estimate specifications of the form:

$$M_{odt} = \exp[\alpha_o + \gamma_d + \delta_t + \beta \text{Dist}_{od}^{\text{Climate}} + \theta \text{Dist}_{od}^{\text{Physical}} + \eta \mathbf{X}'_{od}]\epsilon_{odt} \tag{1}$$

M_{odt} is a measure of migration intensity between the origin and the destination in a given period. We measure genetic connectedness using identity-by-descent (IBD) segments—stretches of DNA shared by two individuals due to common ancestry. Longer segments indicate more recent shared ancestors: an 8 cM segment corresponds to a common ancestor approximately 10–15 generations ago, a 12 cM segment to approximately 8–12 generations ago, and a 16 cM segment to approximately 6–9 generations ago.[4] In our baseline specification, M_{odt} is the count of individual pairs sharing at least one IBD segment of 8 cM or longer—each genetically linked pair represents one migration event connecting the two locations. We show robustness to alternative measures in Table A3, including total centimorgan length of all qualifying segments (which captures both the number of connections and their intensity), the count of qualifying segments (allowing close relatives sharing mul-

[4] Ringbauer et al. (2024) identify 8 cM as the minimum segment length at which the ancIBD method reliably detects IBD in ancient DNA.

tiple segments to contribute more than one), and restriction to longer segment thresholds of 12 and 16 cM. $\text{Dist}_{od}^{Climate}$ is the absolute difference in climatic conditions between the two locations. Our preferred definition is the distance in cumulative growing-degree days above 10°C, which summarizes biologically relevant heat accumulation for plant growth and animal productivity. Degree days aggregate daily temperatures exceeding a meaningful physiological threshold, so that warmer days contribute more while colder days contribute little or nothing. As a result, this measure captures both the intensity and duration of warmth during the growing season and is closely aligned with subsistence constraints emphasized in anthropology and archaeology, as well as with paleoclimate evidence showing that growing-season heat accumulation can evolve independently of seasonal or mean temperatures over the Holocene (Mourshed, 2012; Marsicek et al., 2018).[5]

To address concerns related to the spatial correlation of climate and migration, we flexibly control for geographic distance by including both physical distance between o and d and its square ($\text{Dist}_{od}^{Physical}$). The baseline specification also includes origin fixed effects (α_o), destination fixed effects (γ_d), and 500-year period fixed effects (δ_t). Origin and destination fixed effects absorb persistent differences across locations in population size, mobility propensity, and data coverage, while period fixed effects capture aggregate changes in migration intensity over time. Identification therefore comes from variation in migration flows across destination locations that differ in climatic similarity, holding constant origin-specific, destination-specific, and period-specific factors. Finally, the vector $\mathbf{X}_{od}$ includes absolute differences in precipitation, elevation, and soil characteristics to account for other dimensions of environmental similarity that may independently shape migration costs or subsistence compatibility across locations. Standard errors are clustered at the origin–destination level.

Another potential concern is that migrants from places that were climatically dissimilar moved to areas that were attracting migrants from everywhere else—regardless of climate distance. For instance, over the course of centuries (which is the time span of migration in our context) people could move closer to major emerging urban centers, fresh-water basins, or areas with generally milder climate. A related issue is that our dataset may suffer from sample selection, such that the preservation and discovery of burial sites is related to a location's climate. In both cases, the inclusion of ancestors' and descendants' location cells fixed effects, α_o and α_d, should address these concerns. However, what we cannot rule out is that, after controlling for geographic distance and for descendants' location cell fixed effects, climate distance may be correlated with other variables that independently drive migration patterns. Later we seek to assuage this concern by examining the sensitivity of our estimates to the inclusion of different cell-pair-specific controls, such as soil characteristics

[5]We also show robustness to alternative climate measures, such as growing-season temperature.

and elevation.

4.2 Main Results

Table 2 presents results from equation (1). Column 1 reports a parsimonious specification that includes only distance in cumulative growing-degree days above 10°C. The coefficient is negative and statistically significant, indicating that migration flows decline as growing-season heat differences between origin and destination increase. Column 2 augments this specification by adding winter temperature distance and precipitation distance. The coefficient on growing-degree-day distance remains negative, of similar magnitude, and precisely estimated, suggesting that the effect is not driven by other coarse dimensions of climate. Notably, the coefficient on precipitation distance is also negative and highly significant (-0.016), and—in contrast to the GDD coefficient—remains remarkably stable across all subsequent specifications (-0.008 to -0.010), even after controlling for geographic distance. This stability suggests that water availability represented an ecological constraint on migration that operated independently of spatial proximity.

Column 3 further controls for geographic distance by including both distance and distance squared. As expected, the coefficient on growing-degree-day distance attenuates from -0.796 to -0.258, but remains precisely estimated, indicating that climatic similarity matters over and above simple spatial proximity. Column 4 adds origin, destination, and 500-year period fixed effects, absorbing persistent differences in population size, mobility propensity, and sampling intensity across locations, as well as aggregate changes in migration over time. The coefficient on growing-degree-day distance changes little relative to column 3. Column 5, which we treat as our baseline specification, further includes bilateral controls for elevation and soil characteristics; the estimated effect of growing-degree-day distance remains stable.

In the preferred specification, a difference of 1,000 growing-degree days above 10°C—approximately the sample mean—is associated with a reduction in migration of about 26%. As a benchmark, a difference of 1,000 growing-degree days is equivalent to sustaining a 5°C higher mean daily temperature over a 200-day growing season. From an agronomic perspective, this represents a major change in subsistence possibilities, comparable to the climatic gap between cool-temperate cropping systems such as wheat and warmer temperate systems such as maize, which require on the order of 2,500 growing-degree days.

Beyond climate, soil characteristics represent another dimension of ecological matching that consistently predicts migration flows. The coefficient on soil index distance is negative and highly significant across all specifications that include it (-0.26, SE $= 0.04$), with a magnitude comparable to that of GDD distance. This pattern is consistent with the im-

portance of edaphic knowledge for prehistoric subsistence. Early farmers developed detailed understanding of local soil conditions—which soils retained moisture, which drained well, which required amendment with ash or manure—and this knowledge was difficult to transfer to unfamiliar substrates. Soil pH, organic content, and water-holding capacity vary substantially across Western Eurasia and influence which crops can be cultivated and what yields can be expected. Unlike climate, soil characteristics are highly stable over Holocene timescales, so modern soil data reliably capture the conditions these populations faced. The persistent significance of soil matching, even after controlling for climate and geographic distance, suggests that ecological familiarity extended beyond atmospheric conditions to the substrate itself.

4.3 Robustness Checks

In this section, we assess the robustness of the baseline results by varying both the measurement of climate similarity and the stringency of the fixed-effects structure. Columns 6 and 7 of Table 2 examine sensitivity to alternative climate measures. In column 6, we replace growing-degree-day distance with average summer temperature distance. The estimated coefficient remains negative and statistically significant, indicating that the results are not driven by the specific construction of degree days and continue to point to the importance of growing-season conditions more broadly. In column 7, we further augment the baseline specification by controlling for differences in diurnal temperature range, capturing variation in temperature volatility and extremes; the coefficient on growing-degree-day distance is largely unchanged.

Column 8 introduces origin-by-period and destination-by-period fixed effects, allowing push and pull factors at each location to vary flexibly over time. With these fixed effects, identification comes from within-period differences across destinations that face the same origin, and symmetrically, from within-period differences across origins that face the same destination. In other words, the estimates compare migration from a given origin in a given period toward destinations that differ in climatic similarity, net of any time-varying changes in the overall attractiveness of origins or destinations. Even under this demanding specification, the estimated effect of climate distance remains similar in magnitude.

We further assess robustness along several dimensions. First, Table A3 confirms that results are consistent across all alternative measures of migration intensity described above. Second, we replicate the main results using individual-level data in Table A1, leveraging variation across pairs of individuals rather than aggregated grid cells. The consistency of results across levels of aggregation suggests that the patterns are not artifacts of spatial

binning.

4.4 Mechanisms

Land use. If climate matching reflects the specificity of subsistence technologies, we would expect the effect to vary systematically across populations with different modes of production. Farming societies depend heavily on accumulated thermal time for crop growth, making climate-specific knowledge particularly valuable. Pastoralists, while still reliant on seasonal patterns for grazing and animal husbandry, maintain greater mobility and flexibility. Foragers, by contrast, rely on broader ecological knowledge that may transfer more easily across climatic gradients.

We test this prediction by interacting climate distance with indicators of land use at the origin location. Using historical data on cropland and grazing intensity from the HYDE database (Klein Goldewijk et al., 2017), we classify origin locations as predominantly forager, pastoral, or farming based on the relative intensity of cropland versus grazing. Table 5 presents results from both interaction specifications and subsample analyses.

The results reveal striking heterogeneity across subsistence types. Column 1 reports the baseline specification, while columns 2 and 3 add interactions between climate distance and land use type. The GDD $\times$ Farmer interaction is large and negative (-0.73 to -0.85), indicating that farmers show substantially stronger climate matching than the forager reference group. The GDD $\times$ Pastoral interaction is also negative but smaller in magnitude (-0.44 to -0.55). Columns 4–6 present subsample analyses: foragers show no significant response to GDD distance (coefficient: -0.03), pastoralists show a small and statistically insignificant effect (-0.04), while farmers exhibit strong and precisely estimated climate matching (-0.24).

These patterns are consistent with the interpretation that climate-specific human capital was most binding for agricultural populations. Farmers possessed detailed knowledge of local growing seasons, planting times, and crop varieties that was costly to redeploy in climatically unfamiliar environments. Pastoralists, while still affected by seasonal patterns, maintained greater flexibility through mobility and the adaptability of livestock. Foragers, whose subsistence drew on diverse ecological resources, appear to have been least constrained by climate similarity in their migration decisions. Table A5 in the Appendix presents analogous results using individual-level data.

Precipitation and water availability. The results for precipitation distance reveal a complementary pattern that further illuminates the ecological foundations of climate matching. While growing-degree-day matching is strongest among farmers, precipitation matching

shows the *opposite* heterogeneity: foragers and pastoralists exhibit strong and significant responses to precipitation distance (-0.009 and -0.007, respectively), while farmers show no significant effect (column 3 of Table 5). This pattern is consistent with the distinct water dependencies of different subsistence systems. Foragers relied on predictable water sources that concentrated game and supported plant resources; pastoralists required reliable water and pasture for livestock. Both groups possessed detailed knowledge of seasonal water availability—knowledge that transferred poorly to unfamiliar precipitation regimes. Farmers, by contrast, may have adapted to variable rainfall through irrigation, water storage, or drought-tolerant crop selection, reducing their sensitivity to precipitation matching in migration decisions.

This interpretation aligns with archaeological evidence on the devastating role of drought in prehistoric societies. The 4.2 ka megadrought (c. 2200 BCE) triggered widespread societal disruptions across the Mediterranean and West Asia, including the collapse of the Akkadian Empire and Egypt's Old Kingdom (Weiss, 2017). Paleoclimate evidence documents a 30–50% reduction in precipitation delivered by Mediterranean westerlies during this period, with cascading effects on settlement patterns and population movements. The later Bronze Age collapse (c. 1200 BCE) has similarly been linked to prolonged drought conditions in the Eastern Mediterranean (Kaniewski et al., 2013). More broadly, the persistent and stable effect of precipitation distance in our results—together with its concentration among foragers and pastoralists—suggests that water availability was a distinct axis of ecological constraint, complementing the thermal constraints captured by growing-degree days.

Ecological diffusion: Pollen evidence. If migration facilitated the spread of subsistence practices, we would expect genetic flow to predict subsequent changes in vegetation at destination locations. We test this directly using palynological data from sediment cores across Western Eurasia. Specifically, we measure pollen abundance for cereals and grassland taxa at origin and destination grid cells, interpolating from nearby pollen cores using inverse-distance weighting (restricting to cells within 500 km of a core to ensure reliable interpolation). We then regress the pollen distance between origin (at time t) and destination (at time $t + 500$ years) on genetic flow, controlling for climate distance, geographic distance, and origin, destination, and era fixed effects.

Table 6 presents the results. Columns 1–2 examine cereals pollen, while columns 3–4 examine grassland. In both cases, genetic flow is associated with significantly smaller pollen distance at $t + 500$, indicating that destinations receiving more migrants from a given origin came to resemble that origin's vegetation profile over the subsequent 500 years. For cereals, the coefficient is -0.0013 (SE $= 0.0004$), attenuating slightly to -0.0010 when controlling

for local pollen change at the destination. For grassland, the effect is substantially larger (-0.037, SE $= 0.011$) and similarly robust to controls. These patterns are consistent with migration driving the diffusion of agricultural practices: as populations moved, they brought crops and livestock management techniques that reshaped local vegetation. The stronger effect for grassland may reflect the spread of pastoral systems, which transform landscapes through grazing pressure and the introduction of fodder species.

Cultural group. We also examine heterogeneity across cultural groups by interacting GDD distance with indicators for origin population. Steppe-associated populations—including the Yamnaya, Corded Ware, and Bell Beaker groups—exhibit coefficients close to zero, suggesting that climate similarity played a limited role in structuring their migration. This pattern is consistent with the ecological flexibility and high mobility of pastoral societies, whose subsistence strategies may have been less tightly bound to specific thermal regimes. By contrast, later periods such as Early Modern Europe show the strongest climate matching, potentially reflecting the entrenchment of sedentary agriculture and regionally specialized farming systems. Early farming groups display intermediate effects, while hunter-gatherers show modest but nonzero climate matching—suggesting that even foraging populations were not entirely indifferent to climatic similarity in their movements.

Warming vs cooling. A key advantage of our setting is that it spans nearly 10,000 years, a period marked by substantial and persistent climate change over the Holocene. Paleoclimate reconstructions document multi-century episodes of both warming and cooling, with pronounced regional heterogeneity in timing and magnitude (Marcott et al., 2013). As a result, migration decisions unfolded under very different aggregate climatic regimes, ranging from periods in which growing-season conditions became progressively more favorable to periods in which ecological constraints tightened. This long-run temporal variation allows us to move beyond average effects, and examine whether the role of climate similarity in shaping migration differed systematically across climatic regimes.

We exploit this variation by estimating the baseline specification separately for each 500-year era, allowing the GDD coefficient to vary over time. The results reveal a notable temporal pattern: climate matching emerges around 3500 BCE and peaks around 2500 BCE—a period that coincides with the widespread adoption of agriculture across much of Western Eurasia. Earlier periods (pre-3500 BCE) show weaker or even positive GDD coefficients, suggesting that climate matching was less important during the predominantly foraging era. This pattern is consistent with the idea that warming relaxes growing-season constraints by expanding the set of ecologically viable destinations, thereby reducing the

penalty associated with climate mismatch (Richerson et al., 2001; Dow et al., 2009).

5 Adaptation: Migration in Response to Long-Run Climate Change

As noted above, the period we study was characterized by distinct episodes of warming and cooling over the Holocene. These long-run changes imply that populations were repeatedly exposed to shifts in local climatic conditions rather than to a stable environment. We now examine whether migration operated as an adaptive response to climate change. Specifically, we test whether individuals responded to changes in the climate of their ancestral locations by relocating toward destinations whose climatic conditions partially offset those changes.

We return to the individual level dataset (so we move away from the cell-pair dataset). For each ancestor–descendant pair, we first compute the difference between the paleo-climate reconstructed temperature at the ancestor's location evaluated at the time of the descendant and the temperature at the same location at the time of the ancestor. Positive values indicate periods of local warming, while negative values indicate cooling. We then measure temperature change over space induced by migration by comparing the climatic conditions at the descendant's location to those at the ancestral location, using high-resolution modern climate data. This spatial temperature difference captures whether migration moved individuals toward warmer or cooler environments relative to their place of origin.

Given the granularity over time of our data, we can test whether individuals responded to multi-century periods of warming or cooling with offsetting migration. In other words, did people move to marginally cooler places when the overall climate was warming?

Temperature Change over Time For each pair of individuals (ancestor and descendant), we use Paleo-climate data reconstructions (Osman et al., 2021) to calculate the temperature change over time, which we define as the difference between the temperature at time of the descendant at the ancestor's location (o), and the temperature at the ancestor's location at the time of the ancestor. Formally, this quantity is defined as:

$$\text{Temp Change Over Time}_o = Temp_o^{Descendant} - Temp_o^{Ancestor} \tag{2}$$

Thus, a positive value denotes a period of warming (i.e., the temperature has increased in a given location o).

Temperature Change over Space For each pair of individuals, we define the temperature change over space as the temperature difference between the ancestral location cell (o) and the descendant location cell (d), relying on spatially-granular modern TerraClimate data (Abatzoglou et al., 2018).

$$\text{Temp Change Over Space}_{od} = Temp_d^{TerraClimate} - Temp_o^{TerraClimate} \tag{3}$$

We then regress temperature change over time on variations in temperature, precipitation and elevation across space:

$$\text{Temp Change Over Space}_{od} = \beta \text{Temp Change Over Time}_o + X_{od} + \varepsilon_{od} \tag{4}$$

We report results in Table 3. In Column 1, we regress *Temp Change over Time* on *Temp Change Over Space*. In Column 3, we add ancestor and descendant location cell, and time fixed effects. In Column 5, we add as regressors *Precipitation Change over Space*, on top of a quadratic in distance. Column 2, 4 and 6 replicate – respectively – Columns 1, 3, and 5 by weighting observations by the length of segments greater than 8 cM. In all specifications, we cluster standard errors at the ancestor by descendant location cell by 500-year period level.

In each case, we find a negative effect of temperature change over time on the temperature gradient of moves. In other words, our findings indicate that people move to cooler places during periods of warming. This suggests a potential adaptive response to climate change via migration, whereby individuals offset changes in their own "ancestral" temperature over time by moving towards areas that are climatically more similar to their initial climate.

[STOP HERE – WORK IN PROGRESS]

References

Abatzoglou, John T, Solomon Z Dobrowski, Sean A Parks, and Katherine C Hegewisch (2018) "TerraClimate, a high-resolution global dataset of monthly climate and climatic water balance from 1958–2015," *Scientific data*, 5 (1), 1–12.

Allentoft, Morten E, Martin Sikora, Karl-Göran Sjögren et al. (2015) "Population genomics of bronze age Eurasia," *Nature*, 522 (7555), 167–172.

Anderson, James E and Eric Van Wincoop (2003) "Gravity with gravitas: A solution to the border puzzle," *American economic review*, 93 (1), 170–192.

Anthony, David W. (2007) *The Horse, the Wheel, and Language: How Bronze-Age Riders from the Eurasian Steppes Shaped the Modern World*, Princeton, NJ: Princeton University Press.

Ashraf, Quamrul and Oded Galor (2013) "The 'Out of Africa' Hypothesis, Human Genetic Diversity, and Comparative Economic Development," *American Economic Review*, 103 (1), 1—-46.

Ashraf, Quamrul and Stelios Michalopoulos (2015) "Climatic Fluctuations and the Diffusion of Agriculture," *The Review of Economics and Statistics*, 97 (3), 589–609.

Boyd, Robert, Peter J Richerson, and Joseph Henrich (2011) "The cultural niche: Why social learning is essential for human adaptation," *Proceedings of the National Academy of Sciences*, 108 (supplement_2), 10918–10925.

Butler, Ethan E. and Peter Huybers (2013) "Adaptation of US maize to temperature variations," *Nature Climate Change*, 3 (1), 68–72, 10.1038/nclimate1668.

Castiello, Maria Elena, Emmanuele Russo, Héctor Martínez-Grau, Ana Jesus, Georgina Prats, and Ferran Antolín (2025) "Understanding the Spread of Agriculture in the Western Mediterranean (6th–3rd Millennia BC) with Machine Learning Tools," *Nature Communications*, 16, 678, 10.1038/s41467-024-55541-y.

Crosby, Alfred W (1986) *Ecological Imperialism: The Biological Expansion of Europe, 900-1900*, Cambridge University Press.

Diamond, Jared (1997) *Guns, Germs, and Steel: The Fates of Human Societies*, W. W. Norton.

Dow, Gregory K., Clyde G. Reed, and Nancy Olewiler (2009) "Climate Reversals and the Transition to Agriculture," *Journal of Economic Growth*, 14 (1), 27–53, 10.1007/s10887-009-9038-x.

Fenske, James (2014) "Ecology, trade, and states in pre-colonial Africa," *Journal of the European Economic Association*, 12 (3), 612–640.

Galor, Oded and Omer Moav (2002) "Natural Selection and the Origin of Economic Growth," *The Quarterly Journal of Economics*, 117 (4), 1133–1191, 10.1162/003355302320935007.

Galor, Oded and Ömer Özak (2016) "The Agricultural Origins of Time Preference," *American Economic Review*, 106 (10), 3064–3103, 10.1257/aer.20150020.

Giuliano, Paola and Nathan Nunn (2021) "Understanding cultural persistence and change," *The Review of Economic Studies*, 88 (4), 1541–1581.

Guedes, Jade D'Alpoim and Ethan E. Butler (2014) "Modeling Constraints on the Spread of Agriculture to Southwest China with Thermal Niche Models," *Quaternary International*, 349, 29–41, 10.1016/j.quaint.2014.08.003.

Haak, Wolfgang, Iosif Lazaridis, Nick Patterson et al. (2015) "Massive Migration from the Steppe Was a Source for Indo-European Languages in Europe," *Nature*, 522 (7555), 207–211, 10.1038/nature14317.

Hengl, Tomislav (2018a) "Soil bulk density (fine earth) 10 x kg / m-cubic at 6 standard depths (0, 10, 30, 60, 100 and 200 cm) at 250 m resolution (v0.2)," 10.5281/zenodo.2525665.

——— (2018b) "Soil pH in H2O at 6 standard depths (0, 10, 30, 60, 100 and 200 cm) at 250 m resolution (v0.2)," 10.5281/zenodo.2525664.

Hengl, Tomislav and Surya Gupta (2019) "Soil water content (volumetric %) for 33kPa and 1500kPa suctions predicted at 6 standard depths (0, 10, 30, 60, 100 and 200 cm) at 250 m resolution (v0.1)," 10.5281/zenodo.2784001.

Hengl, Tomislav and Ichsani Wheeler (2018) "Soil organic carbon content in x 5 g / kg at 6 standard depths (0, 10, 30, 60, 100 and 200 cm) at 250 m resolution (v0.2)," 10.5281/zenodo.2525553.

Henrich, Joseph (2004) "Demography and cultural evolution: how adaptive cultural processes can produce maladaptive losses—the Tasmanian case," *American antiquity*, 69 (2), 197–214.

Hersbach, Hans, Bill Bell, Paul Berrisford et al. (2020) "The ERA5 global reanalysis," *Quarterly journal of the royal meteorological society*, 146 (730), 1999–2049.

Kaniewski, David, Elise Van Campo, Joel Guiot, Sabine Le Burel, Thierry Otto, and Cecile Baeteman (2013) "Environmental roots of the Late Bronze Age crisis," *PloS one*, 8 (8), e71004.

Klein Goldewijk, K., A. Beusen, J. Doelman, and E. Stehfest (2017) "Anthropogenic land use estimates for the Holocene – HYDE 3.2," *Earth System Science Data*, 9 (2), 927–953.

Lazaridis, Iosif, Nick Patterson, Alissa Mittnik et al. (2014) "Ancient Human Genomes Suggest Three Ancestral Populations for Present-Day Europeans," *Nature*, 513 (7518), 409–413, 10.1038/nature13673.

Lee, Richard B. and Irven DeVore eds. (1968) *Man the Hunter*, Chicago: Aldine de Gruyter.

Marcott, Shaun A., Jeremy D. Shakun, Peter U. Clark, and Alan C. Mix (2013) "A Reconstruction of Regional and Global Temperature for the Past 11,300 Years," *Science*, 339 (6124), 1198–1201, 10.1126/science.1228026.

Marsicek, Jeremiah, Bryan N. Shuman, Patrick J. Bartlein, Sarah L. Shafer, and Simon Brewer (2018) "Reconciling Divergent Trends and Millennial Variations in Holocene Temperatures," *Nature*, 554 (7690), 92–96, 10.1038/nature25464.

Matranga, Andrea (2024) "The Ant and the Grasshopper: Seasonality and the Invention of Agriculture," *Quarterly Journal of Economics*, 139 (3), 1467–1504.

Michalopoulos, Stelios (2012) "The origins of ethnolinguistic diversity," *American Economic Review*, 102 (4), 1508–1539.

Mourshed, Monjur (2012) "Relationship between Annual Mean Temperature and Degree-Days," *Energy and Buildings*, 54, 418–425, 10.1016/j.enbuild.2012.07.024.

Nicolò, Alessandra, Marco Tabellini, and Charles A. Taylor (2026) "Climates of Conquest: Ecological Imperialism through Climate Matching," Working paper.

Nunn, Nathan (2021) "History as evolution," in *The handbook of historical economics*, 41–91: Elsevier.

Obolensky, Marguerite, Marco Tabellini, and Charles Taylor (2024) "Migration, Climate Similarity, and the Consequences of Climate Mismatch," technical report, National Bureau of Economic Research.

Olsson, Ola (2024) "Paleoeconomics," *Springer Books*.

Osman, Matthew B., Jessica E. Tierney, Jiang Zhu, Robert Tardif, Gregory J. Hakim, Jonathan King, and Christopher J. Poulsen (2021) "Globally resolved surface temperatures since the Last Glacial Maximum," *Nature*, 599 (7884), 239–244, 10.1038/s41586-021-03984-4.

Palamara, Pier Francesco, Todd Lencz, Ariel Darvasi, and Itsik Pe'er (2012) "Length Distributions of Identity by Descent Reveal Fine-Scale Demographic History," *American Journal of Human Genetics*, 91 (5), 809–822, 10.1016/j.ajhg.2012.08.030.

Racimo, Fernando, Jessie Woodbridge, Ralph M. Fyfe, Martin Sikora, Karl-Göran Sjögren, Kristian Kristiansen, and Marc Vander Linden (2020) "The Spatiotemporal Spread of Human Migrations during the European Holocene," *Proceedings of the National Academy of Sciences*, 117 (16), 8989–9000, 10.1073/pnas.1920051117.

Ralph, Peter and Graham Coop (2013) "The Geography of Recent Genetic Ancestry across Europe," *PLOS Biology*, 11 (5), e1001555, 10.1371/journal.pbio.1001555.

Ramachandran, Sohini and Noah A Rosenberg (2011) "A test of the influence of continental axes of orientation on patterns of human gene flow," *American journal of physical anthropology*, 146 (4), 515–529.

Reich, David (2018) *Who we are and how we got here: Ancient DNA and the new science of the human past*, Oxford University Press.

Richerson, Peter J., Robert Boyd, and Robert L. Bettinger (2001) "Was Agriculture Impossible during the Pleistocene but Mandatory during the Holocene? A Climate Change Hypothesis," *American Antiquity*, 66 (3), 387–411, 10.2307/2694241.

Ringbauer, Harald, Yilei Huang, Ali Akbari, Swapan Mallick, Iñigo Olalde, Nick Patterson, and David Reich (2024) "Accurate detection of identity-by-descent segments in human ancient DNA," *Nat. Genet.* 56 (1), 143–151.

Schlenker, Wolfram and Michael J. Roberts (2009) "Nonlinear temperature effects indicate severe damages to U.S. crop yields under climate change," *Proceedings of the National Academy of Sciences*, 106 (37), 15594–15598, 10.1073/pnas.0906865106.

Smerdon, Jason E, Jürg Luterbacher, Steven J Phipps et al. (2017) "Comparing proxy and model estimates of hydroclimate variability and change over the Common Era," *Climate of the Past*, 13 (12), 1851–1900.

Steckel, Richard H (1983) "The economic foundations of East-West migration during the 19th century," *Explorations in Economic History*, 20 (1), 14–36.

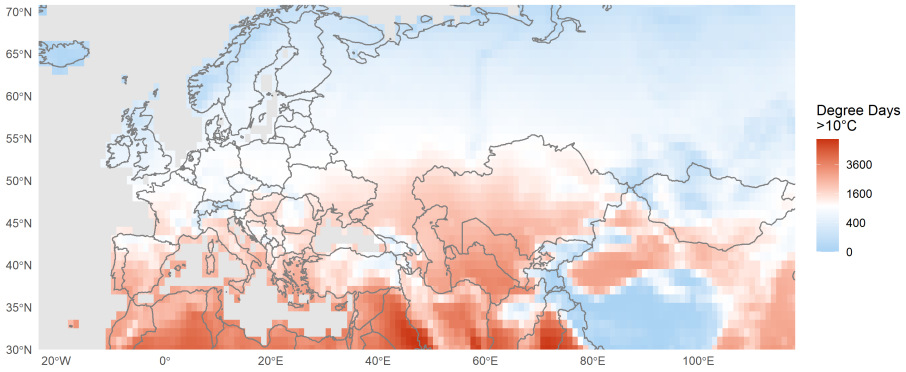
Tierney, Jessica E., Peter B. deMenocal, and Paul D. Zander (2017) "A Climatic Context for the Out-of-Africa Migration," *Geology*, 45 (11), 1023–1026, 10.1130/G39457.1.

Weiss, Harvey (2017) "4.2 ka BP megadrought and the Akkadian collapse," *Megadrought and Collapse: From Early Agriculture to Angkor*, 93–160.

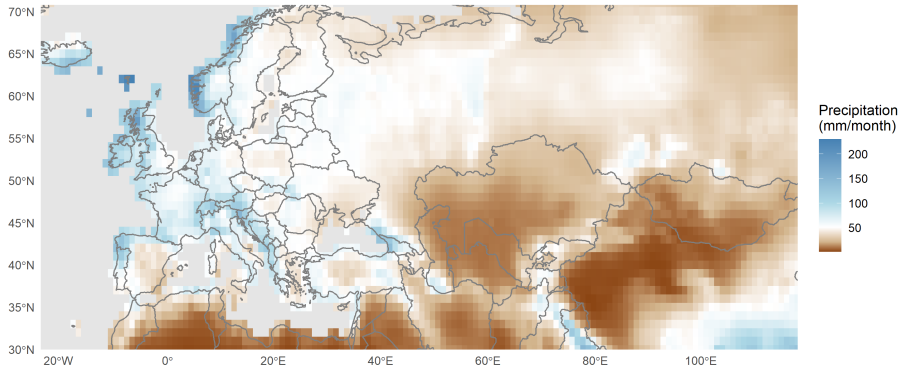
Figures

Figure 1: Modern Climate Variables

(a) Growing Degree Days above 10°C

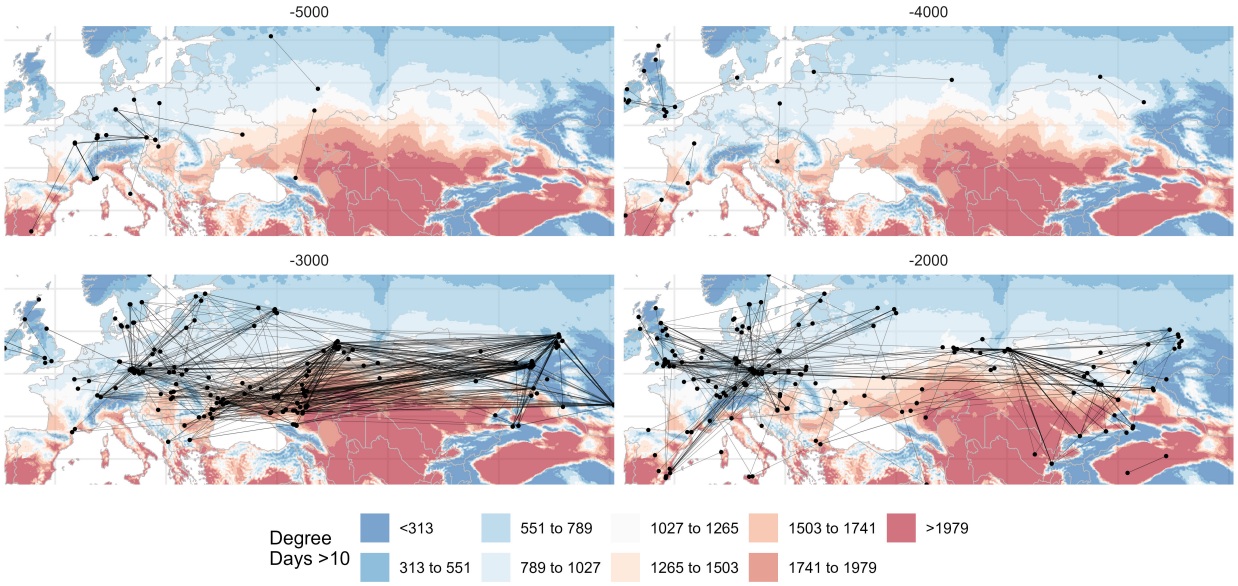


(b) Precipitation



Notes: The figure plots the spatial distribution of modern climate variables at 1° resolution. Panel A shows cumulative growing degree days above 10°C, derived from ERA5 reanalysis data, which captures biologically relevant heat accumulation during the growing season. Panel B shows mean monthly precipitation from TerraClimate (Abatzoglou et al., 2018), averaged over 1960-2000.

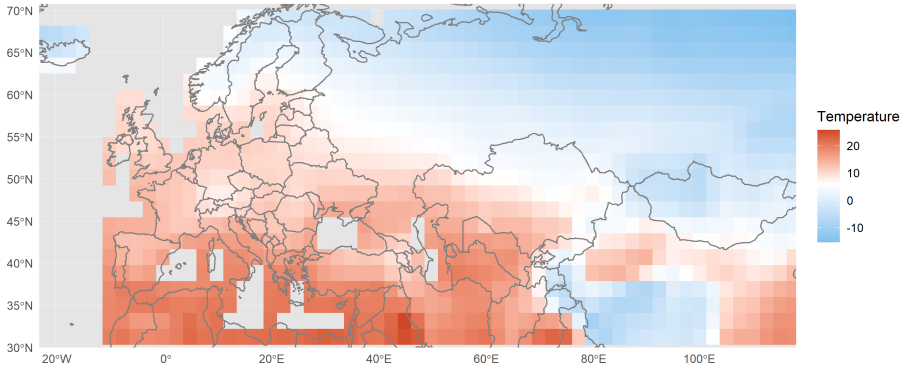
Figure 2: Flows of Individuals



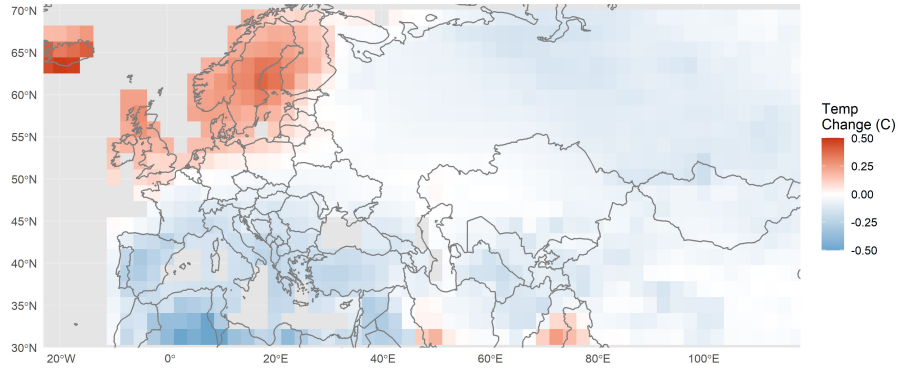
Notes: The figure plots reconstructed flows of individuals in 4 different periods.

Figure 3: Paleoclimate Temperature Reconstructions

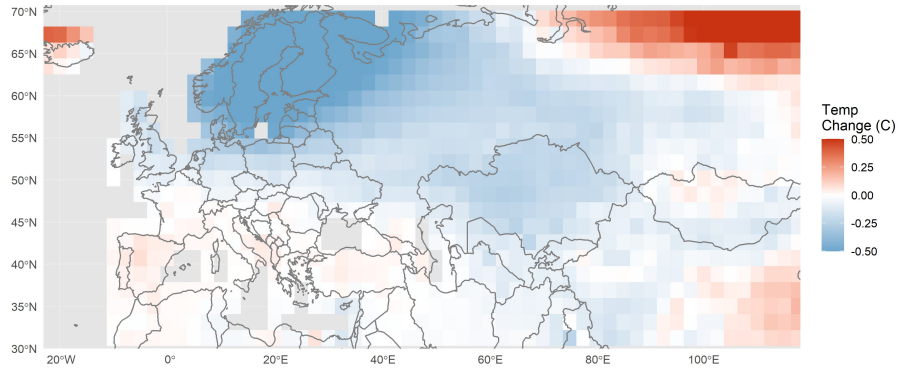
(a) Reconstructed Temperature, 3000 BCE



(b) Temperature Change: 3600 to 3000 BCE



(c) Temperature Change: 1800 to 1200 BCE



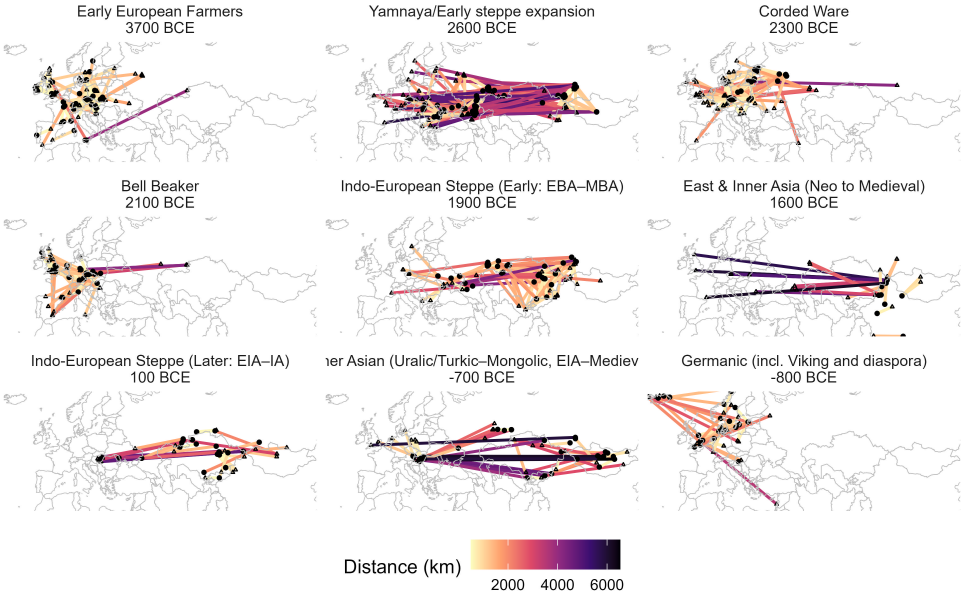
Notes: Panel A shows reconstructed average temperature in 3000 BCE from the marine-based paleoclimate dataset (Osman et al., 2021) at 2.5˚ resolution. Panels B and C plot the change in temperature over 600-year intervals, defined as the difference between the later and earlier period.

Figure 4: Evolution of Average Temperature over Time



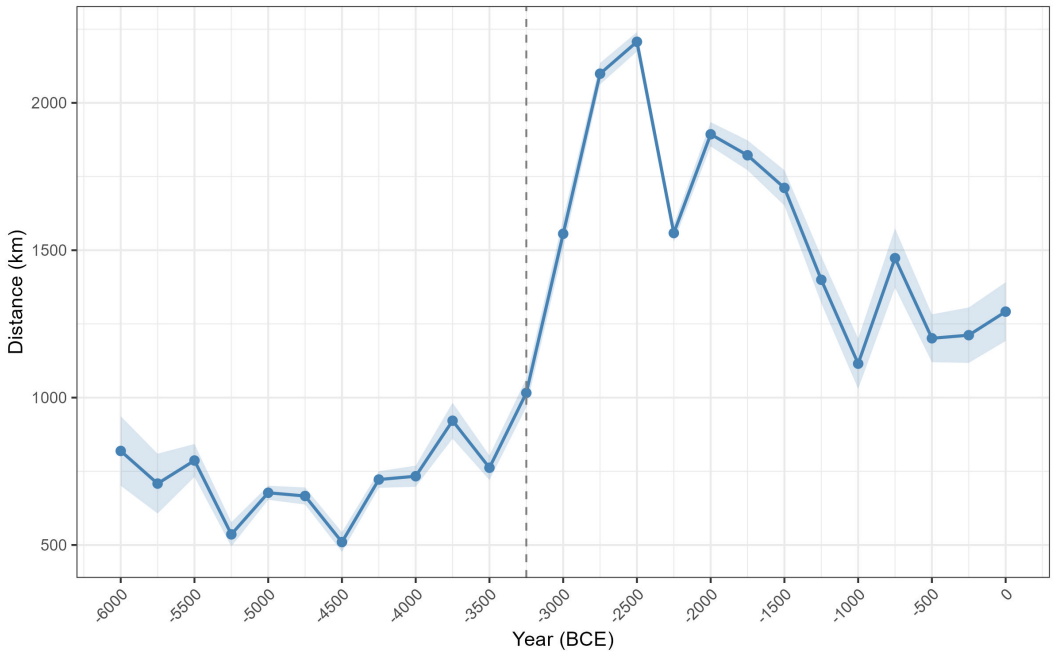
Notes: The figure plots the evolution of (reconstructed) temperature for our sample region of interest over time. Temperature reconstructions are from Osman et al. (2021).

Figure 5: Movements of Major Culture Groups



Notes: The maps show movements of individuals for major cultural groups in our sample. The sample is further restricted to include only pairs of individuals sharing at least one segment greater than 16cM, living at most 500 years apart of each other and whose (geographic) distance is of at least 500km.

Figure 6: Average Distance Between Related Individuals Over Time



Notes: The figure plots the average geographic distance (in kilometers) between genetically related individuals over time, computed at 250-year intervals. Individuals are classified as related if they share at least one IBD segment of 8 cM or longer. The vertical dashed line marks approximately 3250 BCE, corresponding to the adoption of wheel and wagon technology in the Pontic-Caspian steppe region.

Tables

Table 1: Summary Statistics

	Mean	SD	Min	P10	Median	P90	Max	N
IBD Count (8cM)	0.084	1.527	0.000	0.000	0.000	0.000	430.000	875032
IBD Length (12cM)	0.039	1.508	0.000	0.000	0.000	0.000	951.922	875032
IBD Length (8cM)	0.129	2.112	0.000	0.000	0.000	0.000	966.465	875032
GDD Dist.	0.200	0.482	0.000	0.002	0.010	0.665	2.806	873221
Precipitation Dist.	25.905	25.067	0.000	3.291	19.196	55.880	223.053	874895
Distance (000 km)	3.187	2.126	0.042	0.821	2.641	6.306	12.869	875032
Soil Index Dist.	0.723	0.562	0.000	0.109	0.602	1.508	3.735	874895
Elevation Dist.	0.716	0.536	0.000	0.097	0.606	1.497	2.765	874895
Summer Temp. Dist.	4.925	3.951	0.000	0.715	4.020	10.368	30.121	874895
Winter Temp. Dist.	10.102	7.858	0.000	1.331	8.392	21.312	59.702	874895

Table 2: Climate Matching and Migration

Dependent Variable:	Genetic Flow				
Model:	(1)	(2)	(3)	(4)	(5)
Variables					
GDD Dist.	-0.400***	-0.195***	-0.100*	-0.363***	-0.303***
	(0.059)	(0.057)	(0.058)	(0.083)	(0.081)
Winter Temp. Dist.		-0.103***	-0.027***	0.0009	-0.008
		(0.005)	(0.004)	(0.005)	(0.005)
Precipitation Dist.		-0.020***	-0.011***	-0.009***	-0.008***
		(0.001)	(0.001)	(0.001)	(0.001)
Distance (000 km)			-0.920***	-0.850***	-0.727***
			(0.050)	(0.049)	(0.050)
Distance-sq			0.077***	0.082***	0.073***
			(0.005)	(0.007)	(0.007)
Soil Index Dist.					-0.308***
					(0.060)
Elevation Dist.					0.053
					(0.041)
Diurnal Range Dist.					-0.114***
					(0.014)
Fixed-effects					
Orig. gridcell				Yes	Yes
Dest. gridcell				Yes	Yes
Era				Yes	Yes
Fit statistics					
Observations	873,221	873,221	873,221	801,341	797,605
Pseudo R^2	0.003	0.061	0.092	0.461	0.464

*Clustered (grid-cell pair) standard errors in parentheses. ***: p<0.01, **: p<0.05, *: p<0.1*

Notes: Genetic Flow = sum of IBD segment lengths (>8cM). Poisson regression.

Table 3: Climate Change and Adaptation — Individual Level

Dependent Variable:	Temp difference (space)					
	No Dest FE		With Dest FE		+ Precip	
Model:	(1)	(2)	(3)	(4)	(5)	(6)
Variables						
Temp change (400yr window)	-1.51***	-0.935***	-0.384***	-0.298**	-0.366**	-0.327**
	(0.338)	(0.278)	(0.129)	(0.136)	(0.164)	(0.160)
Distance (000 km)	-0.282	0.053	0.008	-0.003	0.024	0.007
	(0.289)	(0.283)	(0.024)	(0.023)	(0.023)	(0.023)
Distance-sq	-0.035	-0.040	-0.003	-0.0002	-0.006	-0.002
	(0.050)	(0.050)	(0.005)	(0.005)	(0.005)	(0.005)
Precip difference (space)					-0.028***	-0.026***
					(0.003)	(0.004)
IBD weighted		Y		Y		Y
Fixed-effects						
Origin grid	Yes	Yes	Yes	Yes	Yes	Yes
Era	Yes	Yes	Yes	Yes	Yes	Yes
Dest grid			Yes	Yes	Yes	Yes
Fit statistics						
Observations	34,378	34,378	34,357	34,357	34,357	34,357
Adjusted R^2	0.422	0.422	0.946	0.946	0.949	0.948

*Clustered (grid-cell pair) standard errors in parentheses. ***: p<0.01, **: p<0.05, *: p<0.1*

Notes: DV is temperature difference between origin and destination. Temp change is 400-year forward change at origin. IBD weighted uses segment lengths as weights.

Table 4: Robustness Checks

Dependent Variables:	Genetic Flow				Count (12cM)	Count (16cM)	Sum Lengths (8cM)
	Baseline	≥100km	Horizontal	Vertical	Count 12cM	Count 16cM	Length 8cM
Model:	(1)	(2)	(3)	(4)	(5)	(6)	(7)
Variables							
GDD Dist.	-0.334***	-0.388***	-0.585***	0.234	-0.716***	-0.953***	-0.409***
	(0.081)	(0.082)	(0.114)	(0.208)	(0.143)	(0.242)	(0.091)
Winter Temp. Dist.	0.0005	0.0003	0.001	0.005	-0.002	-0.0007	0.001
	(0.005)	(0.005)	(0.006)	(0.016)	(0.009)	(0.013)	(0.007)
Precipitation Dist.	-0.009***	-0.009***	-0.010***	-0.0002	-0.015***	-0.017***	-0.012***
	(0.001)	(0.001)	(0.002)	(0.003)	(0.002)	(0.003)	(0.002)
Distance (000 km)	-0.806***	-0.754***	-0.703***	-1.77***	-1.46***	-1.98***	-1.10***
	(0.048)	(0.048)	(0.055)	(0.201)	(0.098)	(0.115)	(0.080)
Distance-sq	0.076***	0.068***	0.061***	0.168**	0.161***	0.228***	0.111***
	(0.007)	(0.007)	(0.008)	(0.071)	(0.014)	(0.016)	(0.011)
Soil Index Dist.	-0.328***	-0.268***	-0.280***	0.006	-0.319***	-0.464***	-0.317***
	(0.060)	(0.060)	(0.072)	(0.078)	(0.085)	(0.102)	(0.067)
Elevation Dist.	0.035	0.054	0.042	-0.086	0.033	-0.074	0.037
	(0.041)	(0.040)	(0.045)	(0.084)	(0.075)	(0.105)	(0.051)
Fixed-effects							
Orig. gridcell	Yes	Yes	Yes	Yes	Yes	Yes	Yes
Dest. gridcell	Yes	Yes	Yes	Yes	Yes	Yes	Yes
Era	Yes	Yes	Yes	Yes	Yes	Yes	Yes
Fit statistics							
Observations	801,341	796,382	649,607	91,155	545,463	359,140	801,341
Pseudo R^2	0.462	0.458	0.485	0.437	0.469	0.456	0.529

*Clustered (grid-cell pair) standard errors in parentheses. ***: p<0.01, **: p<0.05, *: p<0.1*

Notes: Genetic Flow = sum of IBD segment lengths (>8cM). Cols 2–4 restrict sample.

Table 5: Land Use Heterogeneity

Dependent Variable:	Genetic Flow					
Model:	Baseline (1)	+ GDD×Type (2)	+ Precip×Type (3)	Foragers (4)	Pastoral (5)	Farmers (6)
Variables						
GDD Dist.	-0.334***	-1.19***	-1.08***	-0.002	0.458***	0.115
	(0.081)	(0.368)	(0.359)	(0.139)	(0.171)	(0.123)
Winter Temp. Dist.	0.0005	0.026***	0.027***	-0.118***	0.034***	0.032***
	(0.005)	(0.007)	(0.007)	(0.017)	(0.008)	(0.010)
Precipitation Dist.	-0.009***	-0.008***	-0.020***	-0.013***	-0.007***	0.001
	(0.001)	(0.002)	(0.005)	(0.003)	(0.002)	(0.003)
Distance (000 km)	-0.806***	-1.12***	-1.12***	-1.01***	-1.06***	-1.33***
	(0.048)	(0.066)	(0.066)	(0.138)	(0.063)	(0.087)
Distance-sq	0.076***	0.094***	0.093***	0.082***	0.081***	0.107***
	(0.007)	(0.009)	(0.009)	(0.021)	(0.008)	(0.012)
Soil Index Dist.	-0.328***	-0.375***	-0.377***	0.055	-0.251***	-0.499***
	(0.060)	(0.079)	(0.079)	(0.122)	(0.069)	(0.074)
Elevation Dist.	0.035	0.052	0.052	0.015	0.220***	0.070
	(0.041)	(0.058)	(0.058)	(0.091)	(0.073)	(0.061)
Pastoral		-1.13***	-1.33***			
		(0.202)	(0.229)			
Farmer		-1.49***	-1.65***			
		(0.182)	(0.199)			
GDD Dist. × Pastoral		1.82***	1.68***			
		(0.493)	(0.485)			
GDD Dist. × Farmer		1.65***	1.52***			
		(0.446)	(0.434)			
Pastoral × Precipitation Dist.			0.015***			
			(0.005)			
Farmer × Precipitation Dist.			0.014***			
			(0.006)			
Fixed-effects						
Orig. gridcell	Yes	Yes	Yes	Yes	Yes	Yes
Dest. gridcell	Yes	Yes	Yes	Yes	Yes	Yes

Table 6: Ecological Diffusion

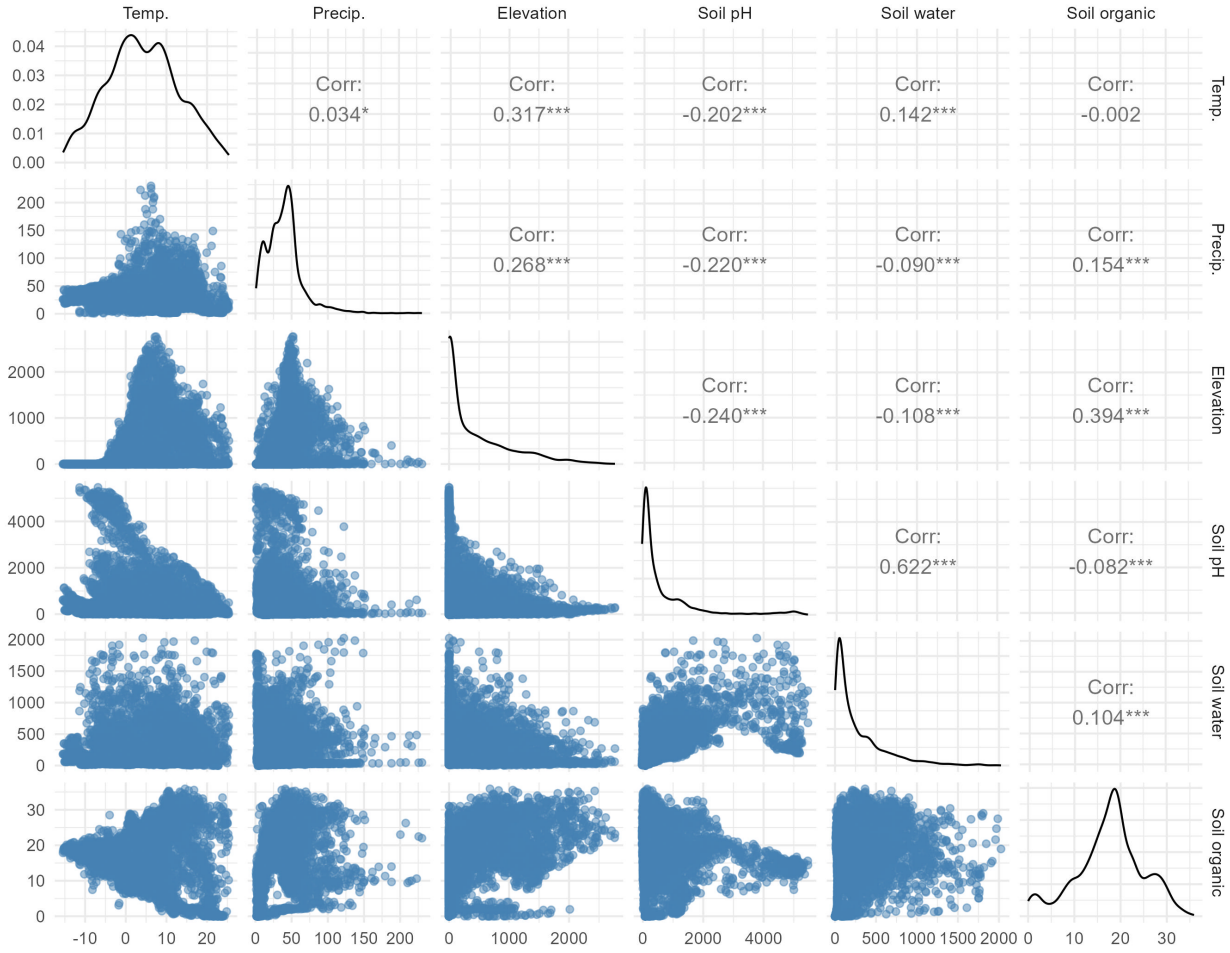
Dependent Variables:	Cereals Pollen Dist.		Grassland Pollen Dist.	
	Cereals	Cereals+Ctrl	Grassland	Grassland+Ctrl
Model:	(1)	(2)	(3)	(4)
Variables				
Genetic Flow	-0.0010**	-0.0006	-0.0371***	-0.0364***
	(0.0004)	(0.0004)	(0.0111)	(0.0109)
Winter Temp. Dist.	-0.0262***	-0.0265***	0.7398***	0.7395***
	(0.0010)	(0.0010)	(0.0114)	(0.0114)
Precipitation Dist.	0.0035***	0.0036***	0.0106***	0.0106***
	(0.0002)	(0.0002)	(0.0039)	(0.0039)
Distance (000 km)	282.3***	278.3***	6,077.0***	6,096.7***
	(10.90)	(10.95)	(159.3)	(159.3)
Distance-sq	-15,644.7***	-14,746.3***	-838,281.7***	-842,726.3***
	(2,069.9)	(2,076.1)	(34,599.1)	(34,621.1)
Soil Index Dist.	0.1405***	0.1429***	-0.9933***	-1.000***
	(0.0067)	(0.0067)	(0.0907)	(0.0907)
Elevation Dist.	0.0614***	0.0625***	2.631***	2.628***
	(0.0047)	(0.0048)	(0.1060)	(0.1061)
Diurnal Range Dist.	-0.0053*	-0.0052*	0.2086***	0.2078***
	(0.0030)	(0.0030)	(0.0374)	(0.0374)
Dest. Pollen Change		0.1742***		-0.1066***
		(0.0061)		(0.0074)
Fixed-effects				
Orig. gridcell	Yes	Yes	Yes	Yes
Dest. gridcell	Yes	Yes	Yes	Yes
Era	Yes	Yes	Yes	Yes
Fit statistics				
Observations	439,913	439,913	439,913	439,913
R^2	0.874	0.875	0.523	0.523

*Clustered (grid-cell pair) standard errors in parentheses. ***: p<0.01, **: p<0.05, *: p<0.1*

Notes: DV is pollen distance between origin (t) and destination (t+500). Sample restricted to cells within 500km of pollen core. OLS regression.

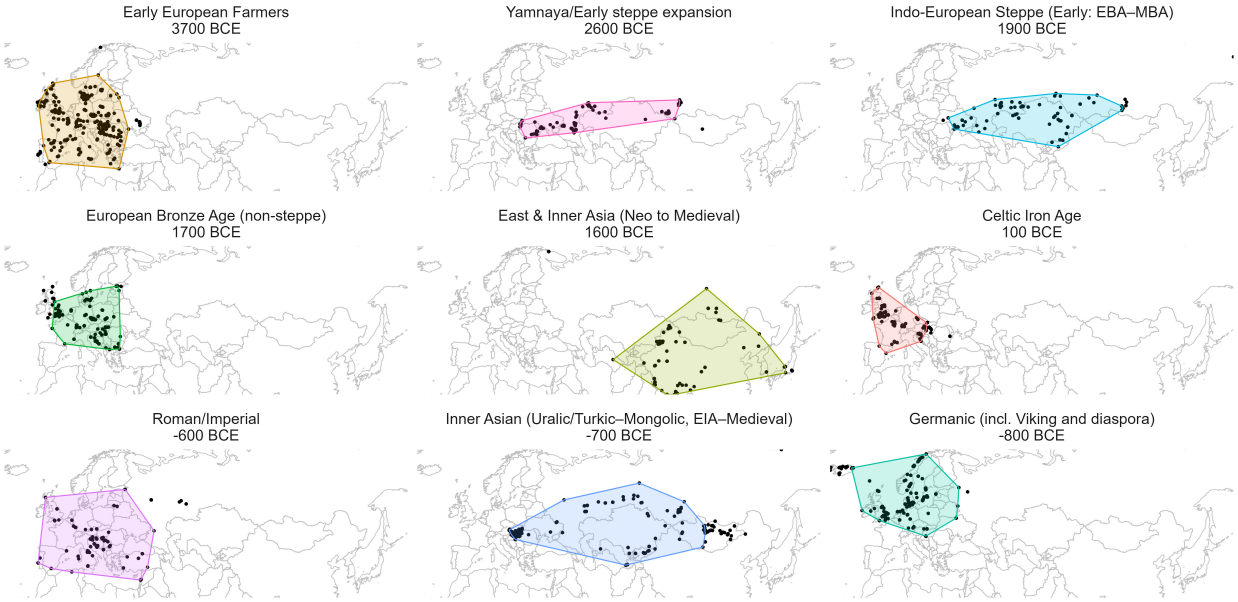
Appendix A - Additional Tables and Figures

Figure A1: Correlation matrix between climate and soil variables



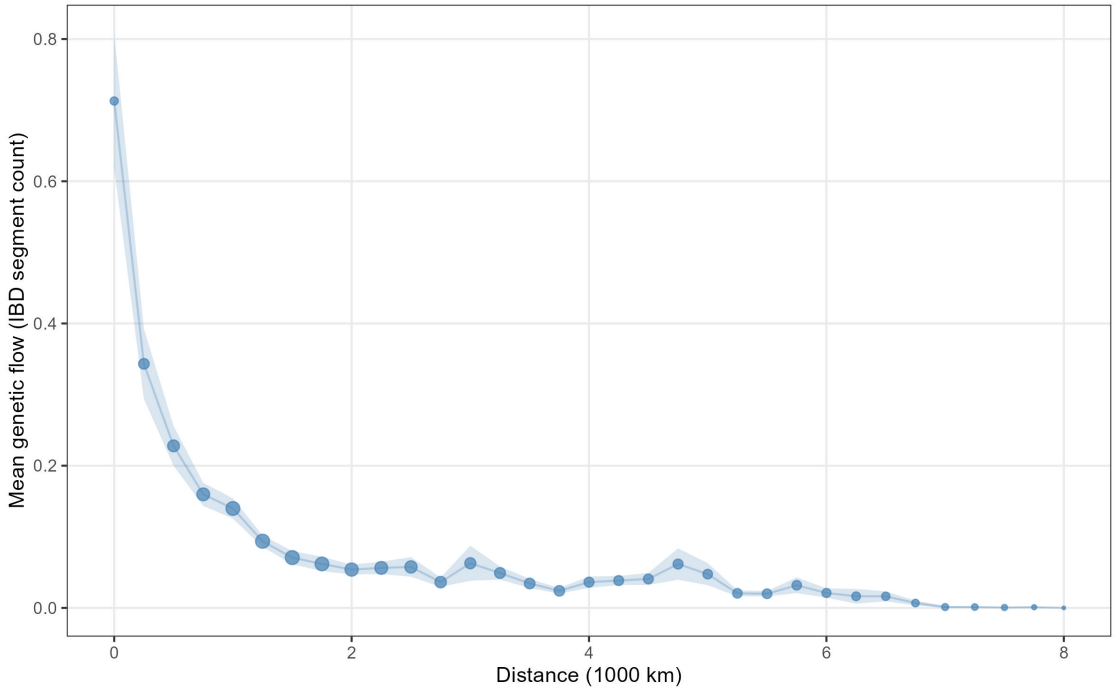
Notes: This figure plots the correlation plots between temperature, precipitation, elevation and the soil variables (soil pH, water holding capacity, organic carbon content, elevation) in each 1˚ x 1˚ cell of our analysis. Climate data come from Abatzoglou et al. (2018) and soil data from Hengl (2018b); Hengl and Gupta (2019); Hengl and Wheeler (2018).

Figure A2: Location of Major Culture Groups



Notes: The maps plot, for each major culture group in our sample, the area where archaeological sites related to that culture are found.

Figure A3: Genetic Flow by Geographic Distance

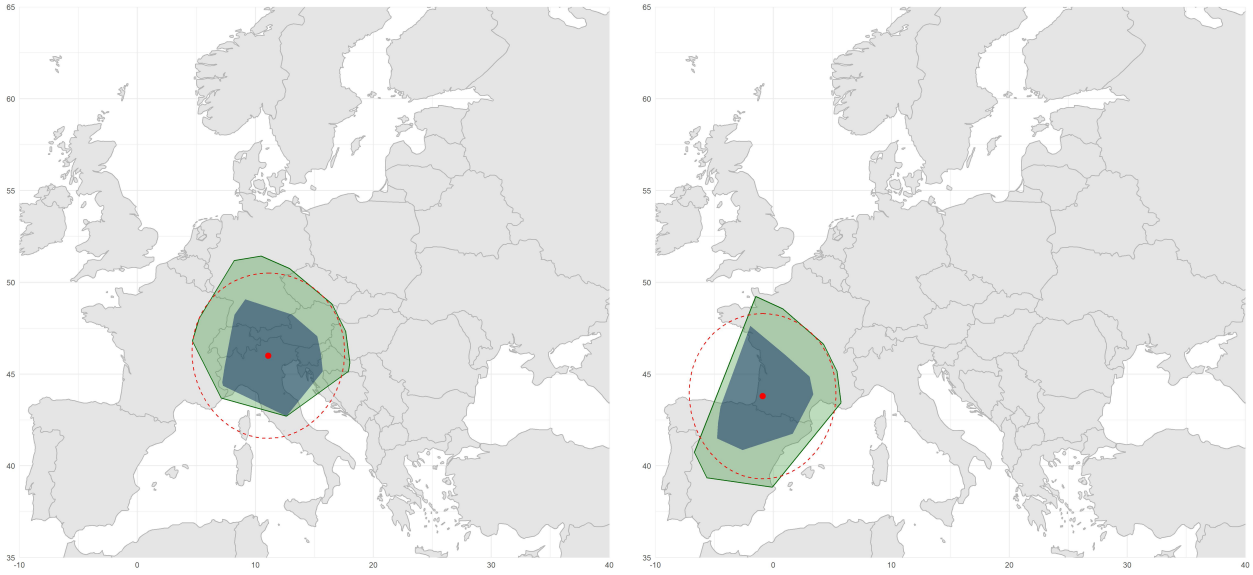


Notes: The figure shows mean genetic flow (IBD segment count $\geq$ 8cM) between grid cell pairs by geographic distance. Points represent 250km distance bins; point size reflects sample size. Shaded ribbon shows 95% confidence interval.

Figure A4: Travel Costs

(a) "Regular" Geography

(b) "Irregular" Geography



Notes: The figures plot spatial differences in travel costs for two random locations in Europe. The blue circle represents an area within 500km from the origin point. The dark blue shaded area is reachable within the by-foot travel cost equivalent of 500 km, while that in dark green the area reachable by the by-horse travel equivalent.

Table A1: Climate Similarity and Migration (Individual-level)

Dependent Variable:	Genetic Flow				
Model:	(1)	(2)	(3)	(4)	(5)
Variables					
GDD Dist.	-0.767***	-0.579***	-0.269***	-0.258***	-0.178***
	(0.071)	(0.066)	(0.056)	(0.055)	(0.053)
Winter Temp. Dist.		-0.073***	-0.004	-0.003	-0.011**
		(0.004)	(0.004)	(0.004)	(0.004)
Precipitation Dist.		-0.012***	-0.007***	-0.007***	-0.006***
		(0.001)	(0.001)	(0.001)	(0.001)
Distance (000 km)			-0.744***	-0.738***	-0.695***
			(0.056)	(0.056)	(0.056)
Distance-sq			0.070***	0.069***	0.072***
			(0.008)	(0.008)	(0.008)
Soil Index Dist.				-0.091***	-0.084***
				(0.016)	(0.015)
Elevation Dist.					-0.025***
					(0.005)
Diurnal Range Dist.					-0.052***
					(0.014)
Fixed-effects					
Orig. gridcell	Yes	Yes	Yes	Yes	Yes
Dest. gridcell	Yes	Yes	Yes	Yes	Yes
Era	Yes	Yes	Yes	Yes	Yes
Fit statistics					
Observations	5,549,643	5,549,643	5,549,643	5,549,643	5,549,643
Pseudo R^2	0.217	0.233	0.243	0.243	0.244

Clustered (geo_pair_ordered) standard-errors in parentheses
*Signif. Codes: ***: 0.01, **: 0.05, *: 0.1*

Table A2: Climate Matching and Migration (2.5° Grid)

Dependent Variable:	Genetic Flow				
Model:	(1)	(2)	(3)	(4)	(5)
Variables					
GDD Dist.	-0.389***	-0.205***	-0.125*	-0.391***	-0.263**
	(0.075)	(0.072)	(0.074)	(0.111)	(0.119)
Winter Temp. Dist.		-0.102***	-0.028***	0.0002	-0.010
		(0.007)	(0.005)	(0.006)	(0.006)
Precipitation Dist.		-0.019***	-0.008***	-0.006***	-0.006***
		(0.002)	(0.002)	(0.002)	(0.002)
Distance (000 km)			-0.901***	-0.765***	-0.622***
			(0.077)	(0.068)	(0.059)
Distance-sq			0.068***	0.068***	0.057***
			(0.008)	(0.009)	(0.008)
Soil Index Dist.					-0.610***
					(0.117)
Elevation Dist.					0.140**
					(0.064)
Diurnal Range Dist.					-0.123***
					(0.020)
Fixed-effects					
Orig. gridcell				Yes	Yes
Dest. gridcell				Yes	Yes
Era				Yes	Yes
Fit statistics					
Observations	362,947	362,947	362,947	335,007	333,598
Pseudo R^2	0.003	0.069	0.108	0.481	0.487

*Clustered (grid-cell pair) standard errors in parentheses. ***: p<0.01, **: p<0.05, *: p<0.1*

Notes: Genetic Flow = sum of IBD segment lengths (>8cM). Coarser grid (2.5°) as robustness check.

Table A3: Climate Matching and Migration – Robustness on the Dependent Variable

Dependent Variables:	Genetic Flow	Sum Lengths (12cM)	Mean Length (12cM)	IBD Count (8cM)
Model:	(1)	(2)	(3)	(4)
Variables				
GDD Dist.	-0.303***	-0.724***	-0.814***	-0.334***
	(0.081)	(0.153)	(0.149)	(0.081)
Winter Temp. Dist.	-0.008	0.004	-0.0006	0.0005
	(0.005)	(0.010)	(0.011)	(0.005)
Precipitation Dist.	-0.008***	-0.016***	-0.016***	-0.009***
	(0.001)	(0.003)	(0.002)	(0.001)
Distance (000 km)	-0.727***	-1.66***	-1.48***	-0.806***
	(0.050)	(0.110)	(0.076)	(0.048)
Distance-sq	0.073***	0.186***	0.155***	0.076***
	(0.007)	(0.015)	(0.010)	(0.007)
Soil Index Dist.	-0.308***	-0.407***	-0.182**	-0.328***
	(0.060)	(0.087)	(0.082)	(0.060)
Elevation Dist.	0.053	0.001	0.095	0.035
	(0.041)	(0.085)	(0.063)	(0.041)
Diurnal Range Dist.	-0.114***			
	(0.014)			
Fixed-effects				
Orig. gridcell	Yes	Yes	Yes	Yes
Dest. gridcell	Yes	Yes	Yes	Yes
Era	Yes	Yes	Yes	Yes
Fit statistics				
Observations	797,605	545,463	545,463	801,341
Pseudo R^2	0.46368	0.51438	0.44697	0.46231

*Clustered (grid-cell pair) standard errors in parentheses. ***: p<0.01, **: p<0.05, *: p<0.1*

Notes: Alternative dependent variables measuring genetic relatedness.

Table A4: Climate Similarity and Migration – Robustness

Dependent Variables:	Genetic Flow (8cM)	Genetic Flow (12cM)	Genetic Flow (8-12cM)	Genetic Flow (8cM)	
Model:	(1)	(2)	(3)	(4)	(5)
Variables					
GDD Dist.	-0.178***	-0.274**	-0.274**	-0.319***	-0.321***
	(0.053)	(0.136)	(0.136)	(0.054)	(0.054)
Winter Temp. Dist.	-0.011**	-0.025**	-0.025**	-0.006	-0.007
	(0.004)	(0.011)	(0.011)	(0.005)	(0.005)
Precipitation Dist.	-0.006***	-0.014***	-0.014***	-0.005***	-0.005***
	(0.001)	(0.004)	(0.004)	(0.001)	(0.001)
Distance (000 km)	-0.695***	-1.61***	-1.61***		
	(0.056)	(0.106)	(0.106)		
Distance-sq	0.072***	0.195***	0.195***		
	(0.008)	(0.015)	(0.015)		
Soil Index Dist.	-0.084***	-0.257***	-0.257***	-0.090***	-0.090***
	(0.015)	(0.035)	(0.035)	(0.016)	(0.016)
Elevation Dist.	-0.025***	-0.010	-0.010	-0.018***	-0.019***
	(0.005)	(0.009)	(0.009)	(0.006)	(0.006)
Diurnal Range Dist.	-0.052***	-0.112***	-0.112***	-0.049***	-0.050***
	(0.014)	(0.043)	(0.043)	(0.015)	(0.015)
Travel Cost				-2.94×10^{-7}	
				(1×10^{-6})	
Travel Cost (horse-adj)					-0.003***
					(0.0002)
Fixed-effects					
Origin grid	Yes	Yes	Yes	Yes	Yes
Dest grid	Yes	Yes	Yes	Yes	Yes
Era	Yes	Yes	Yes	Yes	Yes
Fit statistics					
Observations	5,549,643	4,995,829	4,995,829	5,549,643	5,549,643
Pseudo R^2	0.244	0.490	0.490	0.243	0.243

*Clustered (grid-cell pair) standard errors in parentheses. ***: p<0.01, **: p<0.05, *: p<0.1*

Notes: Genetic Flow = IBD segment indicator. Cols 1–3 vary cM threshold. Cols 4–5 use travel cost instead of distance.

Table A5: Land Use Heterogeneity (Individual-Level)

Dependent Variable:	Genetic Flow				
	Baseline	+ GDD×Type	Foragers	Pastoral	Farmers
Model:	(1)	(2)	(3)	(4)	(5)
Variables					
GDD Dist.	-0.200***	-0.355***	-0.197**	0.063	-0.229***
	(0.054)	(0.098)	(0.096)	(0.071)	(0.066)
Winter Temp. Dist.	-0.008*	-0.009**	-0.047***	-0.001	0.002
	(0.004)	(0.004)	(0.011)	(0.005)	(0.007)
Precipitation Dist.	-0.006***	-0.006***	-0.008***	-0.004**	2.49×10^{-5}
	(0.001)	(0.001)	(0.002)	(0.002)	(0.003)
Geographic Dist.	-0.725***	-0.721***	-1.07***	-0.566***	-0.882***
	(0.054)	(0.053)	(0.093)	(0.070)	(0.075)
Distance-sq	0.072***	0.072***	0.109***	0.050***	0.070***
	(0.008)	(0.008)	(0.012)	(0.010)	(0.012)
Soil Index Dist.	-0.086***	-0.085***	-0.091***	-0.075***	-0.055***
	(0.015)	(0.015)	(0.024)	(0.020)	(0.016)
Elevation Dist.	-0.027***	-0.028***	0.023**	-0.050***	-0.006
	(0.005)	(0.005)	(0.010)	(0.005)	(0.009)
Pastoral		0.013			
		(0.073)			
Farmer		-0.173*			
		(0.090)			
GDD Dist. × Pastoral		0.281***			
		(0.107)			
GDD Dist. × Farmer		0.138			
		(0.117)			
Fixed-effects					
Origin grid	Yes	Yes	Yes	Yes	Yes
Era	Yes	Yes	Yes	Yes	Yes
Dest. grid	Yes	Yes	Yes	Yes	Yes
Fit statistics					
Observations	5,549,643	5,540,626	660,993	1,909,257	2,840,877
Pseudo R^2	0.244	0.244	0.233	0.261	0.232